Research Square

Preprints are preliminary reports that have not undergone peer review.
They should not be considered conclusive, used to inform clinical practice,
or referenced by the media as validated information.

Continuous-Flow Pb(II) Removal by Natural Zeolite: Adsorption, Regeneration, and Reusability in Comparison with a Sodium Alginate–Zeolite Composite

Baigalimaa Togoobaatar
National University of Mongolia
Amgalan Bor
National University of Mongolia
Undral Baatarkhuu
National University of Mongolia
Ochirkhuyag Bayanjargal
National University of Mongolia
Tamiraa Ganbold
tamiraa@num.edu.mn
National University of Mongolia

Research Article

Keywords: Pb(II), natural zeolite, continuous-flow adsorption, fixed-bed column, breakthrough, regeneration, reusability

Posted Date: November 25th, 2026

DOI: https://doi.org/10.21203/rs.3.rs-11315882/v1

License: This work is licensed under a Creative Commons Attribution 4.0 International License.
Read Full License

Additional Declarations: No competing interests reported.

Continuous-Flow Pb(II) Removal by Natural Zeolite: Adsorption, Regeneration, and Reusability in Comparison with a Sodium Alginate–Zeolite Composite

Baigalimaa Togoobaatar, Amgalan Bor, Undral Baatarkhuu, Ochirkhuyag Bayanjargal, Tamiraa Ganbold*
Department of Chemical and Biological Engineering, School of Engineering and Technology, National University of Mongolia, Ulaanbaatar, 14201, Mongolia.
Corresponding authors: tamiraa@num.edu.mn;
ORCID: Tamiraa Ganbold 0000-0001-9965-9208

Abstract
This study provides an integrated process-level assessment of untreated granular natural zeolite for continuous Pb(II) removal, linking particle-size selection with breakthrough behavior, regenerant selection, and repeated fixed-bed reuse. Unlike studies focused primarily on batch equilibrium or material modification, the present work evaluates the trade-off between particle size and column operability, compares natural zeolite with an alginate–zeolite composite under matched flow conditions, and quantifies performance loss during repeated NaCl regeneration. The 1–2 mm zeolite fraction was selected for subsequent column experiments. At 50 mg/L Pb(II) and 10 mL/min, the zeolite showed an experimental adsorption capacity of 130.42 mg/g, compared with 91.69 mg/g for the composite, while the highest capacity of 141.27 mg/g was obtained at 100 mg/L and 10 mL/min. Increasing flow rate and influent concentration accelerated breakthrough. The Yoon–Nelson model effectively described changes in 50% breakthrough time, whereas the Thomas-derived capacity was less reliable under rapid breakthrough at 20 mL/min. Among the tested regenerants, 2% NaCl was more effective than H_2SO_4. After three adsorption–desorption cycles, zeolite capacity decreased from 96.31 to 72.60 mg/g, demonstrating substantial reuse potential.

Keywords: Pb(II), natural zeolite, continuous-flow adsorption, fixed-bed column, breakthrough, regeneration, reusability

Synopsis: This study establishes a practical fixed-bed adsorption and regeneration strategy for repeated Pb(II) removal using natural zeolite, highlighting particle-size selection, breakthrough behavior, and NaCl regeneration rather than relying on material modification or machine-learning optimization.

I. Introduction

Water pollution caused by heavy metals represents one of the most critical environmental challenges worldwide due to their toxicity, persistence, and bioaccumulative nature. Unlike organic pollutants, heavy metals cannot be biodegraded and therefore persist in aquatic ecosystems, soils, and sediments for prolonged periods (Roy et al. 2024; Sahu et al. 2025). Exposure to heavy metals such as lead (Pb), cadmium (Cd), mercury (Hg), and chromium (Cr) is associated with severe health risks, including neurotoxicity, renal dysfunction, cardiovascular diseases, and developmental impairments in children (Emmanuel et al. 2022; Teschke and Xuan 2025). Human activities are major sources of heavy metal contamination, with industrial operations such as mining, metal processing, electroplating, battery manufacturing, and textile production contributing significantly to elevated metal concentrations in surface waters and groundwater. In addition, urban runoff, improper disposal of electronic waste, and

agricultural practices involving contaminated fertilizers further exacerbate heavy metal pollution. Given these concerns, effective remediation strategies are essential to protect human health and aquatic ecosystems (Das et al. 2023; Oladimeji et al. 2024).

Traditional methods for heavy metal removal from water include chemical precipitation, coagulation–flocculation, ion exchange, membrane filtration, and adsorption using activated carbon. While these methods can reduce metal concentration, they have several limitations, including high operational costs, generation of secondary chemical sludge, incomplete removal at low contaminant concentrations, and energy-intensive processing. Consequently, increasing attention has been directed toward the development of cost-effective, sustainable, and environmentally friendly adsorbent materials that can efficiently remove heavy metals, be regenerated for repeated use, and minimize secondary waste. Among these approaches, adsorption has emerged as a preferred method due to its simplicity, high efficiency, and adaptability to continuous treatment systems (Qasem et al. 2021; Fei and Hu 2023).

Zeolites have attracted considerable attention as adsorbents for heavy-metal removal because of their crystalline aluminosilicate framework, cation-exchange capacity, chemical stability, and availability (Rahman et al. 2022). The interconnected $[SiO_4]^{4-}$ and $[AlO_4]^{5-}$ tetrahedra form channels and cavities containing water molecules and exchangeable cations, providing sites for Pb(II) uptake through ion exchange and other surface interactions (Bahmanzadegan and Ghaemi 2025). Adsorption performance is influenced by particle size, surface area, Si/Al ratio, exchangeable-cation composition, and solution chemistry (Velarde et al. 2023). Clinoptilolite is particularly attractive because of its structural stability and affinity for divalent metal cations. However, material properties measured under batch conditions do not by themselves establish suitability for fixed-bed treatment, where particle size and hydraulic behavior can strongly influence performance (Rahman et al. 2022; Alotaibi 2025).

Particle size is an important factor affecting both adsorption performance and hydraulic behavior in continuous-flow systems. Fine zeolite particles are commonly used in adsorption studies because their greater accessible surface area and shorter intraparticle diffusion distances can enhance adsorption kinetics. However, very fine particles are less suitable for fixed-bed columns because they can reduce interparticle void space, increase hydraulic resistance and pressure drop, and promote bed compaction, clogging, and particle loss. Consequently, particle sizes that perform effectively in batch adsorption may not necessarily provide optimal performance under continuous-flow conditions. Larger and more uniform zeolite particles can improve bed permeability and hydraulic stability, although excessively large particles may increase diffusion limitations and reduce adsorption efficiency. Therefore, identifying an appropriate particle-size range is essential for balancing adsorption performance with stable column operation (Zhang et al. 2022; Nakhaei et al. 2023).

Column adsorption provides a more direct assessment of dynamic treatment performance than conventional batch tests, while regeneration determines whether an adsorbent can be used repeatedly without excessive loss of capacity (Eberle et al. 2023; Hu et al. 2024; Milićević et al. 2025). A practical gap therefore remains between demonstrating Pb(II) uptake by natural zeolite and identifying operating conditions that balance adsorption performance, hydraulic stability, and regeneration efficiency in a reusable fixed-bed system. The contribution of the present study is centered on this process-level assessment. Natural zeolite from the Tsagaan Tsav deposit was evaluated at three particle-size ranges (0.45–1, 1–2, and 2–3 mm) to identify a suitable fraction for continuous operation. The selected fraction was then examined under different flow rates and influent Pb(II) concentrations, directly compared with a sodium alginate–zeolite composite under matched operating conditions, and subjected to NaCl and H_2SO_4 regeneration tests. Finally, the best-performing regenerant was evaluated over three consecutive adsorption–desorption cycles. This integrated evaluation links particle-size selection, breakthrough behavior, comparative adsorption capacity, regenerant selection, and repeated column reuse, providing practical information that can be transferred to other granular natural-zeolite fixed-bed systems.

II. Materials and Methods

2.1 Preparation of Reagents and Adsorbent Materials

Lead solutions were prepared by diluting a 1000 mg/L Pb atomic absorption spectrometry (AAS) standard solution to obtain concentrations ranging from 5 to 100 mg/L. For desorption experiments, 2% sodium chloride (NaCl) and sulfuric acid (H_2SO_4) solutions were prepared as regenerants. The adsorbent materials consisted of zeolite collected from the Tsagaantsav deposit in Dornogovi Province, Mongolia, and a composite previously developed in our laboratory. The zeolite was crushed, washed five times with deionized water, dried at room temperature, and sieved into three particle-size fractions: 0.45–1, 1–2, and 2–3 mm. The composite was prepared according to the previously reported method (Munkhbat et al. 2020) by incorporating zeolite particles into a crosslinked sodium alginate matrix to form composite beads. After drying, the Na-alginate/zeolite composite beads (composite) had a diameter of approximately 1–2 mm. The adsorbents were characterized by X-ray diffraction (XRD), X-ray fluorescence (XRF), Fourier-transform infrared spectroscopy (FTIR), scanning electron microscopy (SEM), zeta-potential analysis, and Brunauer–Emmett–Teller (BET) surface-area analysis.

2.2 Column Adsorption

Continuous-flow adsorption experiments were conducted in laboratory-scale fixed-bed glass columns operated in down-flow mode under ambient conditions. The columns had an internal diameter of 1.0 cm and a packed bed height of 3.0 cm. Each column was packed with 1.75 g of natural zeolite or 2.41 g of sodium alginate–zeolite composite. The columns were operated vertically, with influent introduced at the top and effluent collected at the bottom. Pb(II) solutions with initial concentrations of 15, 50, and 100 mg/L were used for the particle-size and influent-concentration experiments, while 5, 10, and 20 mL/min were used to evaluate the effect of flow rate at 50 mg/L. The empty-bed contact time was approximately 14 s at 10 mL/min, 28 s at 5 mL/min, and 7 s at 20 mL/min. For direct comparison of zeolite and composite performance, both materials were tested at 50 mg/L and 10 mL/min. Effluent samples were collected at predetermined intervals and analyzed for Pb(II) concentration using AAS. The normalized effluent concentration (C_t/C_0) was used to evaluate column performance, with lower C_t/C_0 values indicating greater Pb(II) removal. The total amount of lead ion adsorbed and the experimental column adsorption capacity were calculated using a mass-balance approach (Tsai et al. 2016; Futalan and Wan 2022) as follows:

$$q_{total} = \frac{Q}{1000}\int_0^{t_{total}}(C_0 - C_t)dt, \qquad q_e = \frac{q_{total}}{M} \qquad (1)$$

where Q is the flow rate (mL/min), C_0 is the influent lead concentration (mg/L), C_t is the effluent lead concentration at time t (mg/L), t_{total} is the total operating time (min), and M is the mass of adsorbent (g). The effluent concentration was expressed as (C_t), and breakthrough curves were constructed by plotting (C_t/C_0) as a function of operating time. The experimental breakthrough data were analyzed using Thomas and Yoon–Nelson models to evaluate column adsorption kinetics and performance.
Thomas and Yoon–Nelson models were expressed as (Futalan and Wan 2022; Wang et al. 2024):

$$\ln\left(\frac{C_t}{C_0} - 1\right) = \frac{k_{TH}q_0M}{Q} - k_{TH}C_0t \qquad \ln\left(\frac{C_t}{C_0 - C_t}\right) = k_{YN}(t - \tau) \qquad (3)$$

where k_{TH} is the Thomas rate constant, q_0 is the maximum adsorption capacity predicted by the Thomas model, k_{YN} is the Yoon–Nelson rate constant, and τ is the time required for 50% adsorbate breakthrough.

2.3 Regeneration of Adsorbent Materials: Batch and Continuous Desorption

Regeneration experiments were conducted using Pb(II)-loaded adsorbents obtained following adsorption from a 50 mg/L Pb(II) solution. For batch desorption, 0.25 g of Pb(II)-loaded natural zeolite or sodium alginate–zeolite composite was treated with 50 mL of either 2% NaCl or 2% H_2SO_4 solution under gentle agitation for 1, 3, and 5 h. For continuous-column regeneration, Pb(II)-loaded natural zeolite was regenerated by passing 1000 mL of 2% NaCl solution through the column at a flow rate of 5 mL/min. The regenerated zeolite was subsequently reused under the same adsorption conditions for repeated adsorption–desorption cycles. Desorption efficiency was calculated (Rahimi et al. 2026) as follows:

$$Des.eff.[\%] = \frac{m_{des}}{m_{bef.des}} \times 100\% \qquad (4)$$

where m_{des} is the amount of Pb(II) released during desorption, and $m_{bef.des}$ is the total amount of Pb(II) retained on the zeolite immediately before desorption, including residual Pb(II) carried over from the preceding cycle where applicable. Furthermore, statistical analyses were performed using two-way ANOVA followed by Tukey's multiple comparisons test, where appropriate, with statistical significance set at $p < 0.05$; data analysis and graphing were conducted using GraphPad Prism 11.0.0.

III. Results and Discussion

3.1 Material characterization of natural zeolite and Pb(II) loaded zeolite

XRD patterns of untreated and Pb(II)-loaded zeolite showed broadly similar diffraction profiles, with the major reflections retained after adsorption. The untreated zeolite exhibited prominent reflections at approximately 2θ = 9.72°, 22.22°, 29.90°, and 31.86°, corresponding to d-spacings of 9.09, 4.00, 2.99, and 2.81 Å, respectively. Following Pb(II) adsorption, only minor shifts in peak position and d-spacing were observed; for example, the reflection at 22.22° shifted to approximately 22.40°, with the corresponding d-spacing changing from 3.998 to 3.966 Å (Fig.1).

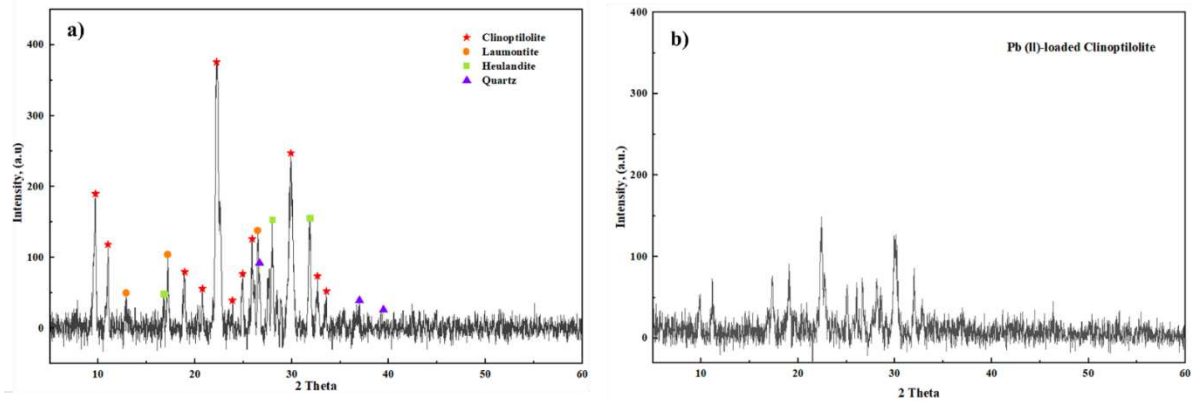

Fig. 1. XRD patterns of untreated zeolite and Pb(II)-loaded zeolite.

Although the characteristic diffraction peaks were retained after Pb(II) adsorption, the relative intensities of several major reflections decreased, particularly those near 22.2°, 29.9°, and 31.9°. These changes indicate a modification of the local structural environment following Pb^{2+} uptake. The observed peak shifts and intensity changes may be associated with interactions of Pb(II) with the zeolite framework and exchangeable cations; however, XRD alone does not establish a specific adsorption mechanism.

XRF analysis showed that the zeolite was composed primarily of Si and Al, together with Na, K, Ca, and Mg (Table 1). Following lead adsorption, the Pb content increased markedly from 0.0011

to 2.59 wt.%, while Na decreased from 2.08 to 1.47 wt.% (~29%). In contrast, the Si and Al contents and the atomic Si/Al ratio (4.55–4.50) remained similar, indicating that the bulk aluminosilicate composition was largely preserved during Pb^{2+} adsorption. The simultaneous Pb enrichment and Na depletion are consistent with a possible contribution from cation-exchange interactions. Similar trends have been reported for Pb(II)-loaded natural zeolites (Uygun et al. 2023, Stepova and Konanets 2024). However, because exchangeable-cation release and cation-exchange capacity were not directly quantified in the present study, the XRF results should be interpreted as supporting rather than conclusive evidence for ion exchange. Overall, the elemental changes indicate substantial Pb uptake while preserving the bulk aluminosilicate composition.
The complete trace-element composition of the untreated and Pb(II)-loaded zeolite samples is provided in Table S1 of the Supplementary Material. The elements directly relevant to the zeolite framework and Pb(II) adsorption are discussed in the main text.

Table 1. Selected elemental composition of natural zeolite before and after Pb(II) adsorption

Elements (wt.%)	***Si***	***Al***	***Na***	***K***	***Ca***	***Mg***	***Fe***	***Pb***	***LOI****
Untreated zeolite	31.15	6.85	2.08	2.6	0.71	0.32	0.69	0.0011	11.41
Pb(II)-loaded zeolite	30.04	6.67	**1.47**	2.69	0.84	0.45	0.92	**2.59**	11.36

**LOI, loss on ignition.*

The FTIR spectra of the raw and Pb(II)-loaded clinoptilolite samples show the characteristic vibrational bands of the aluminosilicate framework. For the raw zeolite, the bands observed at approximately 444, 518, 599, 669, 719, 792, and 1014 cm^{-1} can be attributed to the bending and stretching vibrations of the Si/Al–O framework (Fig. 2). In particular, the band at 1014 cm^{-1} is associated with the asymmetric stretching vibration of Si–O–T (T = Si or Al), which is characteristic of the clinoptilolite framework. After the lead adsorption, these framework-related bands were retained, although slight shifts were observed, including changes from 444 to 447 cm^{-1}, 518 to 513 cm^{-1}, and 599 to 594 cm^{-1}. These changes suggest that Pb(II) adsorption modifies the local chemical environment of the surface and framework oxygen sites without causing substantial disruption of the clinoptilolite structure. The band near 1635 cm^{-1} in the raw zeolite, which shifted to approximately 1625 cm^{-1} after Pb(II) adsorption, is assigned to the H–O–H bending vibration of adsorbed water. The observed shift may reflect changes in the hydration environment associated with Pb(II) adsorption.

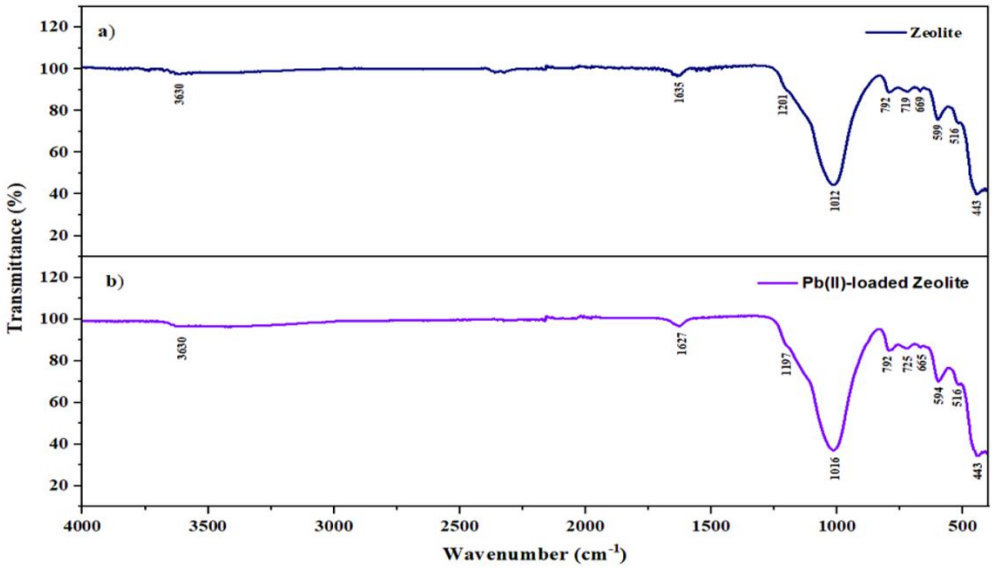

Fig. 2. FTIR spectra of untreated zeolite and Pb(II)-loaded zeolite.

The surface and porosity properties of the zeolite and Pb(II)-loaded zeolite were evaluated. The zeta potential changed from −14.39 mV for the pristine zeolite to +24.75 mV after adsorption. This reversal of surface charge provides evidence of substantial interaction between Pb^{2+} and the zeolite surface and is consistent with uptake at negatively charged surface sites. The BET surface area decreased only slightly from 23.44 to 22.79 m^2/g after adsorption, while the average pore diameter remained nearly unchanged (20.9 to 20.8 nm), indicating that the overall porous structure was largely preserved. Taken together, the XRD, XRF, FTIR, zeta-potential, and BET results show that Pb(II) uptake was accompanied by measurable changes in elemental composition, surface charge, and local chemical environment without substantial alteration of the zeolite framework or textural properties. These results support the occurrence of surface interactions and possible cation exchange during lead uptake, but do not allow the relative contribution of individual mechanisms to be quantified.

The SEM images showed changes in the surface morphology of the natural zeolite after Pb(II) adsorption (Fig. 3). Before adsorption, the zeolite exhibited irregular and angular particles with rough surfaces and relatively distinct interparticle voids.

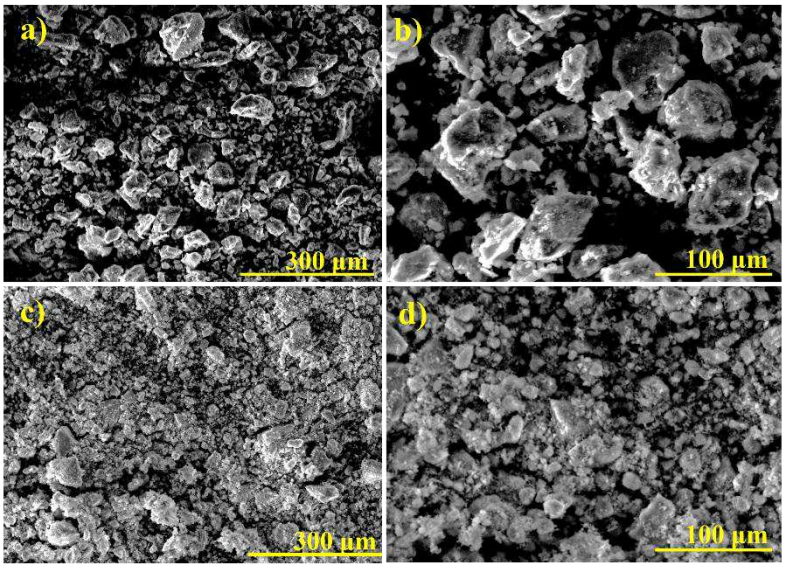

Fig. 3. SEM images of natural zeolite before and after Pb(II) adsorption: (a, b) before adsorption with different magnifications; (c, d) after Pb(II) adsorption with different magnifications.

The particles consisted of a mixture of larger fragments and fine particles, indicating the natural zeolite's heterogeneous nature. After Pb(II) adsorption, the surface appeared relatively more compact and heterogeneous, with increased aggregation of fine particles and less distinct interparticle spaces. Because SEM provides morphological rather than chemical identification, the observed changes are interpreted as evidence of surface modification rather than direct proof of Pb deposition.

3.2 Column adsorption

Breakthrough curves were obtained from fixed-bed column experiments to evaluate the effects of particle size and influent Pb^{2+} concentration on continuous-flow performance. Three particle-size ranges (0.45–1, 1–2, and 2–3 mm) and three influent concentrations (15, 50, and 100 mg/L) were evaluated at a constant flow rate of 10 mL/min. Particle size was the dominant factor affecting the initial breakthrough behavior (Fig, 4). At the initial point, C_t/C_0 increased systematically with particle size, from 0.02–0.04 for 0.45–1 mm particles to 0.45–0.61 for 2–3 mm particles, demonstrating more effective initial Pb^{2+} removal by the smaller particles. The differences between the 0.45–1 and 2–3 mm

fractions were significant at all matched influent concentrations ($p < 0.01$), while the 1–2 and 2–3 mm fractions also differed significantly ($p < 0.05$). At saturation, a similar particle-size-dependent trend was observed, with C/C_0 increasing from 0.08–0.37 for 0.45–1 mm particles to 0.58–0.71 for 2–3 mm particles. Two-way ANOVA confirmed significant effects of both particle size and influent concentration on C_t/C_0, although post hoc analysis indicated that particle size accounted for the more consistent differences among groups. These results show that smaller particles provided more effective initial Pb(II) removal than coarser fractions. The 1–2 mm zeolite fraction was selected for subsequent experiments primarily to enable a direct comparison with the composite, whose beads had a diameter of approximately 1–2 mm. This choice ensured that differences in breakthrough behavior between the two adsorbents could be attributed mainly to material properties rather than particle-size effects.

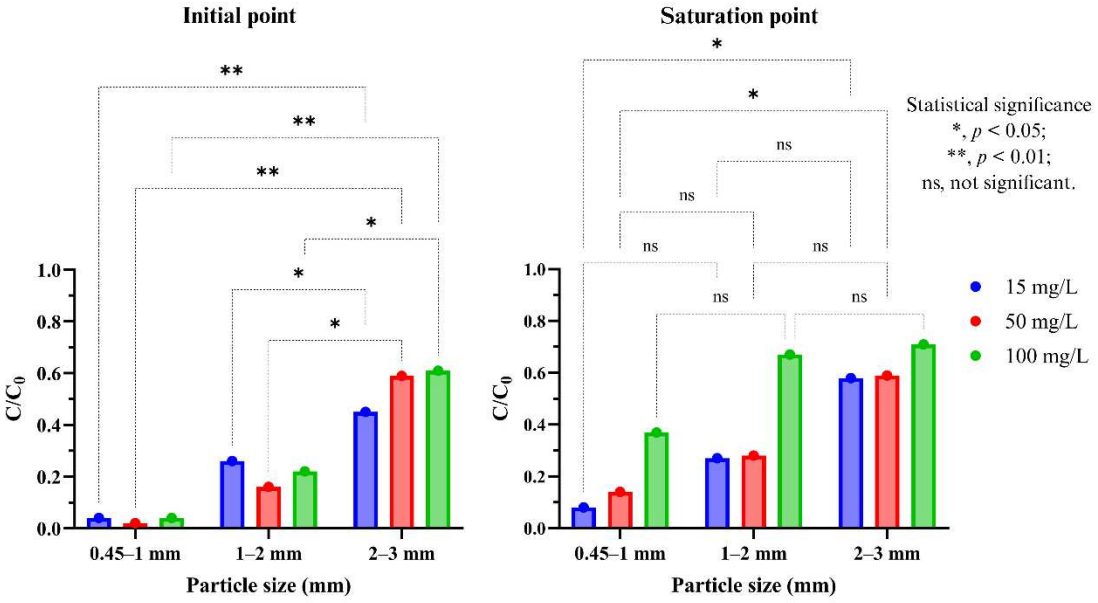

Fig. 4. Effect of zeolite particle size on Pb(II) removal in a continuous fixed-bed column. A) Initial point C/C_0 ratios; B) saturation point C_t/C_0 ratios.

Following particle-size evaluation, the 1–2 mm zeolite fraction was selected for subsequent continuous-flow experiments using 1.75 g of zeolite. The effects of flow rate and Pb(II) concentration on breakthrough behavior were evaluated by monitoring C_t/C_0 as a function of operating time (Fig. 5). At 50 mg/L, increasing the flow rate from 5 to 20 mL/min resulted in a progressively steeper breakthrough curve and earlier increase in C_t/C_0. At 5 mL/min, C_t/C_0 increased gradually from 0.05 at 25 min to approximately 0.90 at 1500 min, whereas at 10 mL/min it reached 0.90 at approximately 1250 min. At 20 mL/min, C_t/C_0 reached approximately 0.92 within 750 min. This behavior is consistent with reduced residence time at higher flow rates, which limits contact between Pb(II) and available adsorption sites and results in earlier breakthrough.

In addition to flow rate, influent Pb(II) concentration affected the breakthrough behavior at a constant flow rate of 10 mL/min. Increasing the influent concentration from 15 to 100 mg/L resulted in an earlier increase in (C_t/C_0) and a shorter effective operating period of the column (Fig. 5). At 15 mg/L, (C_t/C_0) increased gradually and reached approximately 0.54 at 1000 min and 0.79 at 1950 min. In comparison, at 50 mg/L, (C_t/C_0) reached 0.90 at approximately 1250 min, while at 100 mg/L it reached 0.95 within 950 min. Thus, higher influent Pb(II) concentrations promoted earlier breakthrough and more rapid progression toward saturation (Fig. 5).

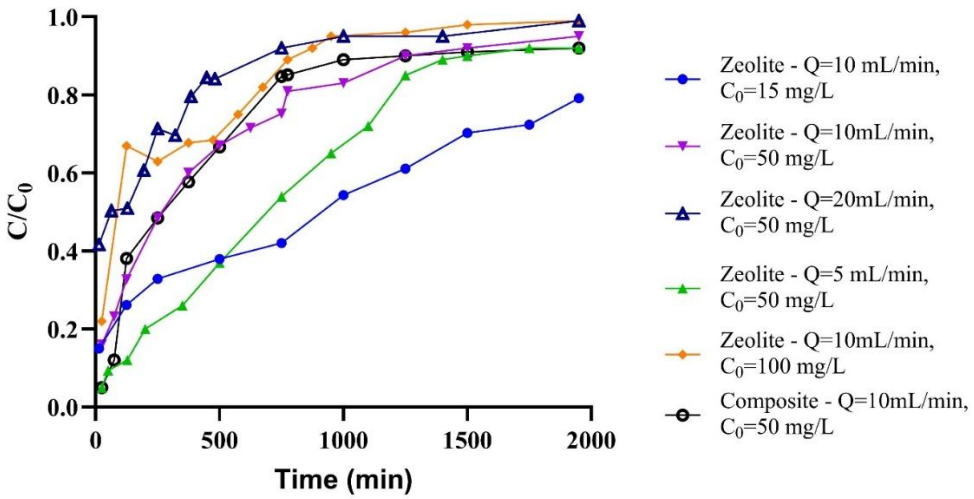

Fig. 5. Breakthrough curves for Pb(II) removal using zeolite and composite under continuous-flow conditions.

The observed trends are consistent with the combined effects of residence time and Pb(II) loading rate. Higher flow rates reduce contact time, while higher influent concentrations increase the rate at which adsorption sites are occupied. Accordingly, fixed-bed performance depends on balancing mass-transfer driving force with sufficient residence time for effective Pb(II) uptake.

3.3 Kinetic models on breakthrough curve

Because the sodium alginate–zeolite composite was previously developed for lead adsorption in our laboratory (Munkhbat et al. 2020), it was included here as a reference material to determine whether incorporation of zeolite into an alginate matrix provides an advantage under continuous-flow conditions. The comparison was performed using the same particle-size range, influent concentration, and flow rate (Fig. 5). For direct comparison, both adsorbents had a particle size of 1–2 mm and were evaluated at an influent Pb(II) concentration of 50 mg/L and a flow rate of 10 mL/min. The columns contained 1.75 g of zeolite or 2.41 g of composite. The composite exhibited a lower initial C/C_0 value than zeolite (0.05 vs. 0.16 at 25 min), indicating greater initial Pb(II) removal. However, the breakthrough profiles became increasingly similar as column operation progressed. At 500 min, C/C_0 values were approximately 0.67 for both adsorbents, while both reached approximately 0.90 at 1250 min. At 750 min, zeolite maintained a lower C/C_0 value (0.75) than the composite (0.85), indicating greater Pb(II) removal at this intermediate stage. Thus, under the tested conditions, the natural zeolite achieved comparable or better breakthrough performance despite the lower packed mass, indicating that incorporation into the sodium alginate matrix did not provide a clear dynamic-performance advantage. The breakthrough data obtained using the selected 1–2 mm zeolite fraction were further analyzed to determine the total amount of Pb(II) adsorbed (q_{total}), equilibrium capacity (q_e), and kinetic parameters describing continuous-column performance. The experimental adsorption results are summarized in Table 2, while the Thomas and Yoon–Nelson models are presented in Table 3.

Model fits for the different flow rates and influent Pb(II) concentrations are provided in the Supplementary Material (Figure S1). Under identical operating conditions (Q = 10 mL/min and C_0= 50 mg/L), the natural zeolite exhibited a higher experimental adsorption capacity than the composite (130.42 versus 91.69 mg/g). However, the total amounts of lead ions adsorbed were relatively similar (228.23 and 220.98 mg, respectively), because the packed-bed composite mass was higher. For natural zeolite at 50 mg/L, the experimental capacity increased from 96.31 mg/g at 5 mL/min to 130.42 mg/g at 10 mL/min and then decreased to 115.18 mg/g at 20 mL/min, indicating a balance between mass-

transfer driving force and residence time. At 10 mL/min, increasing the influent concentration from 15 to 50 and 100 mg/L increased the experimental capacity from 79.68 to 130.42 and 141.27 mg/g, respectively, consistent with a stronger concentration gradient and higher lead ion loading.

Table 2. Experimental Pb(II) adsorption performance of zeolite and composite

Adsorbent	Flow rate	Initial Concentration	Total Adsorbed Ion	Equilibrium capacity
	Q (mL/min)	C_0 (mg/L)	q_{total} (mg)	q_e (mg/g)
Zeolite	5	50	168.55	96.31
	10	50	228.23	130.42
	20	50	201.56	115.18
	10	15	139.45	79.68
	10	100	247.23	141.27
Composite	10	50	220.98	91.69

The Thomas and Yoon–Nelson models were applied to describe the breakthrough behavior and evaluate the dynamic adsorption performance of the zeolite column (Table 3). For the natural zeolite, both models generally provided good linear fits to the breakthrough data, with R^2 values ranging from 0.90 to 0.96; however, the reliability of the model-derived capacity parameter depended on the extent of the experimentally captured breakthrough region. At C_0 = 50 mg/L, the Thomas model predicted adsorption capacities (q_0) of 205.67, 102.46, and 13.54 mg/g at flow rates of 5, 10, and 20 mL/min, respectively. The markedly low q_0 value obtained at 20 mL/min should be interpreted cautiously. At this highest flow rate, breakthrough occurred rapidly, with C_t/C_0 increasing to approximately 0.92 within 750 min, resulting in a limited breakthrough transition region for reliable estimation of the Thomas capacity parameter. Thus, the Thomas-derived q_0 of 13.54 mg/g does not represent the experimentally determined adsorption capacity of 115.18 mg/g under this condition. Nevertheless, the 20 mL/min experiment was useful for demonstrating the strong effect of flow rate on breakthrough behavior.

The Yoon–Nelson model provided a clear description of the effect of operating conditions on breakthrough time. At C_0= 50 mg/L, the 50% breakthrough time (τ) decreased from 787.07 min at 5 mL/min to 358.61 and 57.79 min at 10 and 20 mL/min, respectively. Thus, although the Thomas-derived capacity at 20 mL/min was considered unreliable, the Yoon–Nelson τ value clearly demonstrated the pronounced acceleration of breakthrough with increasing flow rate. Similarly, at a constant flow rate of 10 mL/min, increasing C_0 from 15 to 50 and 100 mg/L reduced τ from 945.79 to 358.61 and 105.25 min, respectively. These results demonstrate that both higher flow rate and higher influent Pb(II) concentration accelerated the progression toward 50% breakthrough, consistent with the breakthrough curves presented in Figure 5.

Table 3. Thomas and Yoon–Nelson model parameters for Pb(II) adsorption in continuous-flow columns.

Adsorbent	**Experimental condition**		**Thomas Model**			**Yoon–Nelson Model**		
	Q	C_0	k_{Th}	q_0	R^2	k_{YN}	τ	R^2
	mL/min	mg/L	mL/(mg·min)	mg/g		1/min	min	
Zeolite	5	50	6.12×10^{-5}	205.67	0.95	0.0028	787.07	0.95
	10	50	4.60×10^{-5}	102.46	0.90	0.0023	358.61	0.90
	20	50	5.85×10^{-5}	13.54	0.93	0.0024	57.79	0.93
	10	15	9.39×10^{-5}	80.60	0.96	0.0014	945.79	0.96
	10	100	3.18×10^{-5}	52.89	0.92	0.0028	105.25	0.92
Composite	10	50	5.00×10^{-5}	90.28	0.72	0.0025	435.16	0.72

For the composite tested at Q = 10 mL/min and C_0 = 50 mg/L, the model fits were weaker (R^2 = 0.72) than those obtained for the natural zeolite (R^2 = 0.90). Nevertheless, the Thomas model predicted an adsorption capacity of 90.28 mg/g, which was close to the experimental value of 91.69 mg/g. The Yoon–Nelson model gave a τ value of 435.16 min, compared with 358.61 min for the natural zeolite, indicating a slower approach to 50% breakthrough under these conditions. The natural zeolite achieved its highest experimental adsorption capacity of 141.27 mg/g at C_0 = 100 mg/L and Q = 10 mL/min. Overall, the model results support the observed effects of flow rate and influent concentration on column breakthrough behavior. In particular, the Yoon–Nelson model was useful for quantifying the time required to reach 50% breakthrough across the tested operating conditions, whereas the Thomas-derived capacity parameter should be interpreted with caution when the breakthrough transition is too rapid to provide a sufficiently broad fitting region.

3.4 Regeneration and reusability of the zeolite and zeolite–alginate composite

Following the column adsorption experiments conducted at an influent Pb(II) concentration of 50 mg/L and a flow rate of 10 mL/min, Pb(II)-loaded zeolite and composite were subjected to batch desorption using 2% NaCl and 2% H_2SO_4 as regenerants.

For each experiment, 0.25 g of Pb(II)-loaded adsorbent was treated with 50 mL of regenerant for 1, 3, and 5 h. The Pb(II) concentration in the regenerant solution was measured by AAS. For natural zeolite regenerated with 2% NaCl, the Pb(II) concentration increased from 65.18 mg/L after 1 h to 79.34 mg/L after 3 h and 89.50 mg/L after 5 h. In contrast, regeneration with 2% H_2SO_4 resulted in Pb(II) concentrations of only 3.17–3.99 mg/L over the same period.

The substantially greater desorption obtained with NaCl indicates that chloride-based regeneration was more effective for releasing Pb(II) retained by the natural zeolite under the tested conditions. This behavior is consistent with previous reports showing effective regeneration of Pb(II)-loaded zeolites using chloride-based regenerants, including NaCl and KCl (Turan et al. 2005; Katsou et al. 2011; Senila and Cadar 2024). The low dissolved Pb(II) recovery observed with H_2SO_4 may reflect not only limited desorption but also possible formation of sparingly soluble $PbSO_4$; therefore, this mechanism should be considered cautiously because precipitation was not directly evaluated in the present study.

The composite exhibited considerably lower Pb(II) desorption than the natural zeolite with both regenerants. For the composite regenerated with 2% NaCl, the Pb(II) concentration in the 50 mL regenerant increased from 1.75 mg/L after 1 h to 3.47 mg/L after 3 h and 5.10 mg/L after 5 h, corresponding to 0.35, 0.69, and 1.02 mg Pb/g adsorbent, respectively. Regeneration with 2% H_2SO_4 resulted in Pb(II) concentrations of 0.60–0.75 mg/L (0.12–0.15 mg Pb/g). The substantially lower desorption from the composite may be associated with stronger Pb(II) retention and/or reduced accessibility of Pb(II) within the alginate–zeolite matrix. Partial structural degradation of the composite was also observed during NaCl treatment, further limiting its suitability for repeated regeneration under the tested conditions. Although no visible degradation was observed during H_2SO_4 treatment, the very low lead ion release indicates poor regeneration efficiency. Although studies specifically addressing Pb(II) desorption from zeolite–alginate composites remain limited, regeneration has been demonstrated for related alginate-based adsorbents. (Chiew et al. 2016) reported more than 90% Pb(II) desorption from calcium-alginate and alginate–halloysite beads using 0.10 M HNO_3, with successful reuse over multiple adsorption–desorption cycles. Similarly, a composite membrane regenerated using 0.1 M HCl for Cu^{2+} adsorption retained more than 80% removal efficiency after five cycles (Yang et al. 2026). These studies indicate that the regeneration performance of alginate-based adsorbents depends strongly on both matrix composition and regenerant chemistry.

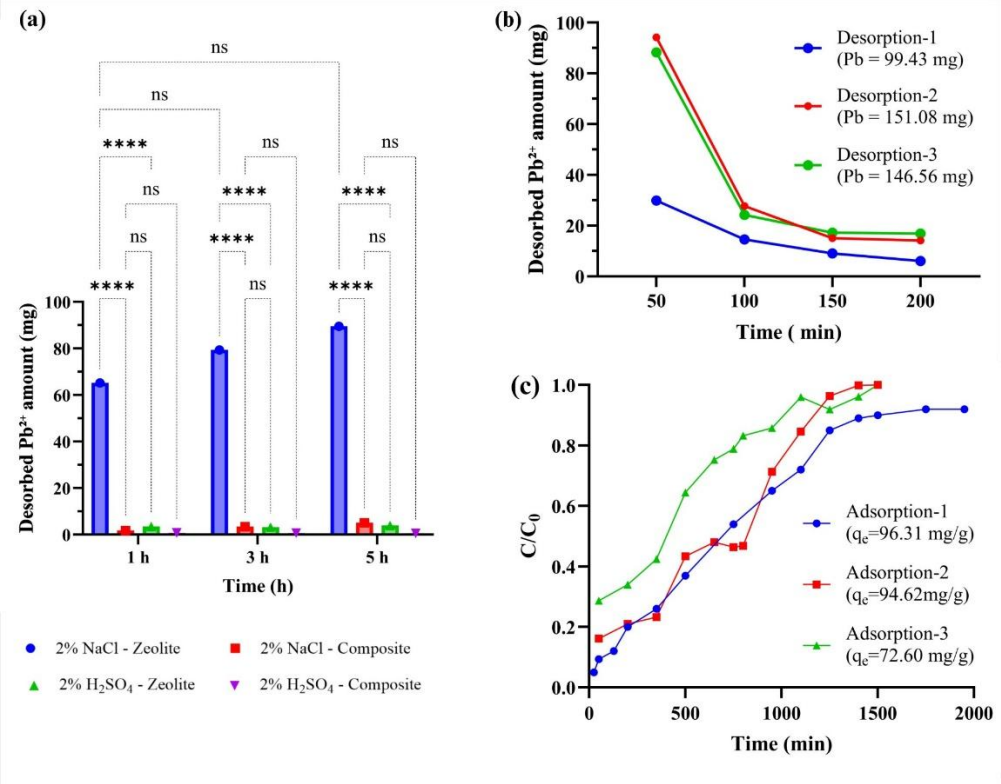

Fig. 6. Desorption, regeneration, and reuse performance of Pb(II)-loaded zeolite and composite.

Based on the substantially higher Pb(II) desorption obtained with 2% NaCl, which was selected for subsequent continuous-column regeneration of the natural zeolite. The regenerability of the 1–2 mm zeolite fraction was evaluated over three consecutive adsorption–desorption cycles. Each adsorption cycle was conducted at 50 mg/L and 5 mL/min, followed by regeneration with 1000 mL of 2% NaCl at the same flow rate. The regenerated zeolite was then reused under the same adsorption conditions. The corresponding breakthrough and desorption profiles are presented in Figures 6b and 6c.

During the first adsorption cycle, the normalized effluent concentration (C_t/C_0) increased from 0.05 at 25 min to 0.54 at 750 min and approximately 0.92 at 1950 min, giving an experimental adsorption capacity (q_e) of 96.31 mg/g. After the first regeneration, the second adsorption cycle exhibited a generally similar breakthrough profile, with C_t/C_0 increasing from 0.16 at 50 min to approximately 1.0 at 1500 min. The corresponding $q_e$was 94.62 mg/g, representing approximately 98% of the initial adsorption capacity and indicating that most of the adsorption performance was preserved after one regeneration cycle. A more pronounced decline was observed during the third adsorption cycle. C_t/C_0 increased from 0.29 at 50 min to 0.64 at 500 min, 0.79 at 750 min, and approximately 1.0 at 1500 min, while the experimental capacity decreased to 72.60 mg/g, approximately 75% of the initial value. The earlier breakthrough and lower capacity indicate a gradual loss of effective adsorption performance following repeated regeneration, which may reflect incomplete lead ion desorption and reduced accessibility of active sites.

The breakthrough data were further evaluated using the Thomas and Yoon–Nelson models to assess changes in column performance after repeated regeneration (Table S3 and Figure S2A, B). The Thomas model predicted adsorption capacities (q_0) of 205.67, 173.80, and 144.99 mg/g for the first, second, and third cycles, respectively. Although the predicted $q_0$values decreased progressively with repeated regeneration, they remained higher than the corresponding experimental q_e values. In addition, the Thomas model showed a weaker fit for the second cycle (R^2 = 0.74) than for the first and third cycles

(R^2 = 0.95 and 0.94, respectively). Therefore, the model-derived q_0 values should be interpreted as fitted dynamic parameters rather than direct measures of the experimentally achieved adsorption capacity. The Yoon–Nelson model showed a consistent decrease in the half-saturation time (τ), from 787.07 min in the first cycle to 564.59 and 357.79 min in the second and third cycles, respectively. The progressive reduction in τ indicates that the column reached 50% breakthrough increasingly earlier during repeated reuse, consistent with the experimentally observed changes in the breakthrough profiles. The model provided good fits for the first and third cycles (R^2 = 0.95 and 0.94, respectively), whereas the second-cycle fit was lower (R^2 = 0.74).

Continuous-column regeneration released total Pb(II) amounts of 99.43, 151.08, and 146.56 mg during the first, second, and third regeneration cycles, respectively. Pb(II) release was highest during the initial stage of each regeneration step and gradually decreased with increasing desorption time, suggesting rapid release of more readily desorbed Pb(II) followed by slower release of more strongly retained Pb(II). When residual Pb(II) carried over from the preceding adsorption cycle was included in the mass balance, the calculated desorption efficiencies were 58.8%, 64.1%, and 69.3%, respectively. Thus, substantial Pb(II) desorption was maintained during repeated NaCl regeneration, although complete restoration of the initial adsorption performance was not achieved.

Taken together, the batch desorption results identified 2% NaCl as a more effective regenerant than 2% H_2SO_4 for Pb(II)-loaded natural zeolite, while the zeolite composite showed substantially lower desorption and limited structural stability during NaCl treatment. Repeated NaCl regeneration allowed the natural zeolite to retain substantial Pb(II) adsorption capability over three adsorption–desorption cycles. The adsorption capacity remained nearly unchanged after the first regeneration, decreasing from 96.31 to 94.62 mg/g, but declined to 72.60 mg/g in the third cycle. The accompanying decrease in Yoon–Nelson half-saturation time confirmed progressively earlier breakthrough during reuse. These results demonstrate the feasibility of NaCl regeneration for repeated continuous-flow Pb^{2+} removal while also showing that regeneration losses accumulate with repeated cycling.

IV. Conclusion

This study demonstrated the potential of natural zeolite for continuous-flow Pb(II) removal and repeated use following regeneration. Characterization results indicated that the zeolite structure and textural properties were largely preserved after Pb(II) adsorption, while changes in Pb and Na contents were consistent with a possible contribution of cation-exchange interactions. In column experiments, particle size, flow rate, and influent Pb(II) concentration strongly affected breakthrough behavior. The 1–2 mm zeolite fraction was used for the comparative column experiments to match the particle size of the composite beads (approximately 1–2 mm). Under these matched conditions, natural zeolite exhibited a higher experimental adsorption capacity than the composite. Under identical conditions of 50 mg/L Pb(II) and 10 mL/min, natural zeolite showed a higher experimental adsorption capacity than the sodium alginate–zeolite composite (130.42 vs. 91.69 mg/g). Among the tested regenerants, 2% NaCl was more effective than 2% H_2SO_4 for Pb(II) desorption from natural zeolite. After three adsorption–desorption cycles, the experimental adsorption capacity decreased from 96.31 to 72.60 mg/g, while the Yoon–Nelson breakthrough time progressively decreased, indicating gradual loss of column performance during reuse. Nevertheless, the zeolite retained substantial adsorption capacity after repeated regeneration. Overall, the results highlight natural zeolite as a promising reusable adsorbent for continuous-flow Pb(II) removal, with NaCl regeneration providing a practical approach for extending adsorbent use.

Author contribution. BT – Writing original draft, performing the experiments; AB – Formal analysis, writing – review; UB – Formal analysis, methodology; OB – Visualization, review, conceptualization; TG - Writing – review and editing, Supervision, Methodology.

Funding. This work was funded by the project P2025-5031 for Fundamental and Applied Research at the National University of Mongolia.

Data availability. All data generated or analyzed during this study are included in this paper.

Conflict of interest. The authors declare that they have no known competing financial interests or personal relationships that could have appeared to influence the work reported in this paper.

References

Alotaibi AM (2025) An Overview of Zeolites: From Historical Background to Diverse Applications. Molecules 30:4036. https://doi.org/10.3390/molecules30204036

Bagotia N (2025) Regeneration strategies for exhausted adsorbents used in water treatment - A critical review. J Water Process Eng 69:106560. https://doi.org/10.1016/j.jwpe.2024.106560

Bahmanzadegan F, Ghaemi A (2025) A comprehensive review on novel zeolite-based adsorbents for environmental pollutants. J Hazard Mater Adv 17:100617. https://doi.org/10.1016/j.hazadv.2025.100617

Chiew CSC, Yeoh HK, Pasbakhsh P, et al (2016) Stability and reusability of alginate-based adsorbents for repetitive lead (II) removal. Polym Degrad Stab 123:146–154. https://doi.org/10.1016/j.polymdegradstab.2015.11.022

Das S, Sultana KW, Ndhlala AR, et al (2023) Heavy Metal Pollution in the Environment and Its Impact on Health: Exploring Green Technology for Remediation. Environ Health Insights 17:11786302231201259. https://doi.org/10.1177/11786302231201259

Eberle S, Schmalz V, Börnick H, Stolte S (2023) Natural Zeolites for the Sorption of Ammonium: Breakthrough Curve Evaluation and Modeling. Molecules 28:. https://doi.org/10.3390/molecules28041614

Emmanuel UC, Chukwudi MI, Monday SS, Anthony AI (2022) Human health risk assessment of heavy metals in drinking water sources in three senatorial districts of Anambra State, Nigeria. Toxicol Rep 9:869–875. https://doi.org/10.1016/j.toxrep.2022.04.011

Fei Y, Hu YH (2023) Recent progress in removal of heavy metals from wastewater: A comprehensive review. Chemosphere 335:139077. https://doi.org/10.1016/j.chemosphere.2023.139077

Futalan CM, Wan M-W (2022) Fixed-Bed Adsorption of Lead from Aqueous Solution Using Chitosan-Coated Bentonite. Int J Environ Res Public Health 19:2597. https://doi.org/10.3390/ijerph19052597

Hu Q, Yang X, Huang L, et al (2024) A critical review of breakthrough models with analytical solutions in a fixed-bed column. J Water Process Eng 59:105065. https://doi.org/10.1016/j.jwpe.2024.105065

Katsou E, Malamis S, Tzanoudaki M, et al (2011) Regeneration of natural zeolite polluted by lead and zinc in wastewater treatment systems. J Hazard Mater 189:773–786. https://doi.org/10.1016/j.jhazmat.2010.12.061

Milićević S, Martinović S, Todorović D, Milošević V (2025) Zeolite fixed-bed system enhanced with recirculation for improved copper ion removal from wastewater: Kinetic models and comparison with batch system. Miner Eng 231:109441. https://doi.org/10.1016/j.mineng.2025.109441

Munkhbat D, Ganbold T, Naranbaatar A, et al (2020) Pb(II)Adsorption of Composite Alginate Beads Containing Mesoporous Natural Zeolite. J Nanosci Nanotechnol 20:5267–5275. https://doi.org/10.1166/jnn.2020.18530

Nakhaei M, Heidarian MH, Vatanpour V, Rezaei K (2023) Evaluation the feasibility of using clinoptilolite as a gravel pack in water wells for removal of lead from contaminated groundwater. Environ Sci Pollut Res 30:4653–4668. https://doi.org/10.1007/s11356-022-22519-6

Oladimeji TE, Oyedemi M, Emetere ME, et al (2024) Review on the impact of heavy metals from industrial wastewater effluent and removal technologies. Heliyon 10:e40370. https://doi.org/10.1016/j.heliyon.2024.e40370

Qasem NAA, Mohammed RH, Lawal DU (2021) Removal of heavy metal ions from wastewater: a comprehensive and critical review. Npj Clean Water 4:36. https://doi.org/10.1038/s41545-021-00127-0

Rahimi V, Samet A, Pimentel CH, et al (2026) Dual-stage treatment of waste printed circuit boards for Cu2+, Pb(II), and Zn2+ recovery: A precipitation-adsorption hybrid process. Sep Purif Technol 414:139797. https://doi.org/10.1016/j.seppur.2026.139797

Rahman ROA, El-Kamash AM, Hung Y-T (2022) Applications of Nano-Zeolite in Wastewater Treatment: An Overview. Water 14:. https://doi.org/10.3390/w14020137

Roy B, Bhunia B, Bandyopadhyay TK, et al (2024) Water Pollution by Heavy Metals and Their Impact on Human Health. In: Handbook of Water Pollution. John Wiley & Sons, Ltd, pp 333–352

Sahu P, Patel AR, Pandey A, et al (2025) Assessment of heavy metal ion toxicity in wastewater: A comprehensive review. Inorganica Chim Acta 585:122751. https://doi.org/10.1016/j.ica.2025.122751

Senila M, Cadar O (2024) Modification of natural zeolites and their applications for heavy metal removal from polluted environments: Challenges, recent advances, and perspectives. Heliyon 10:e25303. https://doi.org/10.1016/j.heliyon.2024.e25303

Stepova K, Konanets R (2024) Clinoptilolite- and glauconite-based sorbents for lead removal from natural waters. J Environ Eng Landsc Manag 32:191–200. https://doi.org/10.3846/jeelm.2024.21831

Teschke R, Xuan TD (2025) Heavy Metals Like Aluminum, Arsenic, Cadmium, Chromium, Copper, Iron, Lead, Manganese, Mercury, Nickel, and Zinc Polluting the Drinking Water: Their Individual Health Hazards. Int J Mol Sci 26:11656. https://doi.org/10.3390/ijms262311656

Tsai W-C, de Luna MDG, Bermillo-Arriesgado HLP, et al (2016) Competitive Fixed-Bed Adsorption of Pb(II), Cu(II), and Ni(II) from Aqueous Solution Using Chitosan-Coated Bentonite. Int J Polym Sci 2016:1608939. https://doi.org/10.1155/2016/1608939

Turan M, Mart U, Yüksel B, Çelik MS (2005) Lead removal in fixed-bed columns by zeolite and sepiolite. Chemosphere 60:1487–1492. https://doi.org/10.1016/j.chemosphere.2005.02.036

Uygun O, Güven R, Çakal GÖ (2023) Adsorptive removal of stable and radioactive Pb(II)isotopes from aqueous solution using bentonite, zeolite and perlite: characterization, isotherm and thermodynamic studies. Clay Miner 58:195–209. https://doi.org/10.1180/clm.2023.18

Velarde L, Nabavi MS, Escalera E, et al (2023) Adsorption of heavy metals on natural zeolites: A review. Chemosphere 328:138508. https://doi.org/10.1016/j.chemosphere.2023.138508

Wang Q, Liang D, Yang Y, et al (2024) A study on a fixed-bed for Pb(II)removal by modified alkaline lignin-sodium alginate composite hydrogel. RSC Adv 14:23483–23494. https://doi.org/10.1039/d4ra02975e

Yang L, Yang Y, Zhu Y, et al (2026) Fabrication of a Recyclable Sodium Alginate-Zeolite/Glutaraldehyde (SA-HZ/GA) Composite Adsorption Membrane and Its Efficient Removal of Cu(II). J Appl Polym Sci 143:e70756. https://doi.org/10.1002/app.70756

Zhang Y, Wang F, Cao B, et al (2022) Simultaneous removal of Pb and MTBE by mixed zeolites in fixed-bed column tests. J Environ Sci 122:41–49. https://doi.org/10.1016/j.jes.2021.10.009

Zeolite Application in Wastewater Treatment - Luciano Fernandes de Magalhães, Gilberto Rodrigues da Silva, Antônio Eduardo Clark Peres, Muhammad Raziq Rahimi Kooh, 2022. https://journals.sagepub.com/doi/10.1155/2022/4544104. Accessed 5 Oct 2026

Supplementary Files

This is a list of supplementary files associated with this preprint. Click to download.

- Baigalaamanuscriptsupplementary.docx